

Novel electronic structure induced by a highly strained oxide interface with incommensurate crystal fields

H. W. Ou,^{1,2} J. F. Zhao,^{1,2} Y. Zhang,^{1,2} B. P. Xie,^{1,2} D. W. Shen,^{1,2} Y. Zhu,¹ Z. Q. Yang,¹ J. G. Che,¹ X. G. Luo,³ X. H. Chen,³ M. Arita,⁴ K. Shimada,⁴ H. Namatame,⁴ M. Taniguchi,⁴ C. M. Cheng,⁵ K. D. Tsuei,⁵ and D. L. Feng^{1,2,*}

¹Department of Physics, Surface Physics Laboratory (National Key Laboratory), Fudan University, Shanghai 200433, P. R. China

²Advanced Materials Laboratory, Fudan University, Shanghai 200433, P. R. China

³Hefei National Laboratory for Physical Sciences at Microscale and Department of Physics, University of Science and Technology of China, Hefei, Anhui 230026, P. R. China

⁴Hiroshima Synchrotron Radiation Center and Graduate School of Science, Hiroshima University, Hiroshima 739-8526, Japan.

⁵National Synchrotron Radiation Research Center, and Department of Physics, National Tsing-Hua University, Hsinchu 30077, Taiwan, Republic of China

(Dated: November 4, 2018)

The misfit oxide, $\text{Bi}_2\text{Ba}_{1.3}\text{K}_{0.6}\text{Co}_{2.1}\text{O}_y$, made of alternating rocksalt-structured [BiO/BaO] layers and hexagonal CoO_2 layers, was studied by angle-resolved photoemission spectroscopy. Detailed electronic structure of such a highly strained oxide interfaces is revealed for the first time. We found that under the two incommensurate crystal fields, electrons are confined within individual sides of the interface, and scattered by umklapp scattering of the crystal field from the other side. In addition, the high strain on the rocksalt layer raises its chemical potential and induces large charge transfer to the CoO_2 layer. Furthermore, a novel interface effects, the interfacial enhancement of electron-phonon interactions, is discovered. Our findings of these electronic properties lay a foundation for designing future functional oxide interfaces.

PACS numbers: 71.27.+a, 73.20.-r, 79.60.-i

Oxide interfaces have attracted much attention for the emergence of novel phenomena [1, 2, 3, 4, 5, 6, 7]. For example, high conductivity [1] and even superconductivity [2] were discovered at the interface between two insulators, LaAlO_3 and SrTiO_3 ; ferromagnetism was discovered in the superlattice of two antiferromagnets, LaCrO_3 and LaFeO_3 [3]; and gigantic thermoelectric power at the $\text{SrTiO}_3/\text{SrTi}_{0.8}\text{Nb}_{0.2}\text{O}_3$ interface was discovered five times higher than the bulk material[8]. Clearly, it provides opportunities for promising applications: one may be able to make oxide heterostructure devices with desired physical properties[9]. A thorough understanding of the microscopic processes at the oxide interface is the first step toward designing functional heterostructures. Particularly, it is crucial to find out the electronic behavior at oxide interfaces, *e.g.*, how the electron bands react to two competing, and sometimes incommensurate periodic potentials [10] on both sides of the interface; and how they react to strain, and peculiar phonon structures at the interface [6, 11]. The answers to these questions would lead to the understanding of the charge transfer process, the insulator-metal transitions, and anomalous transport behavior of the interfaces[4, 5, 12].

Angle resolved photoemission spectroscopy (ARPES) is one of the most powerful techniques for studying electronic structure of solids and thin films. Pioneering angle-integrated photoemission experiments have been conducted on pulsed-laser deposited oxide interfaces[13, 14, 15, 16]. However, because the interface is buried far underneath the surface, and the mean free path of photoelectrons is very short, photoemission signals from the interface are very weak, which forbids high resolution and momentum resolved measurements. The recent synthesized misfit oxide single crystals provide an alternative solution[17, 18]. Since each unit cell of a misfit ox-

ide is usually composed of two kinds of oxide layers with distinct space group symmetries, it resembles a very clean artificial oxide heterostructure and suitable for photoemission experiments. For example, each formula unit of misfit cobaltites, which are known for their anomalously large thermoelectric power, consists of several rocksalt-type MO layers ($M=\text{Ca}$,

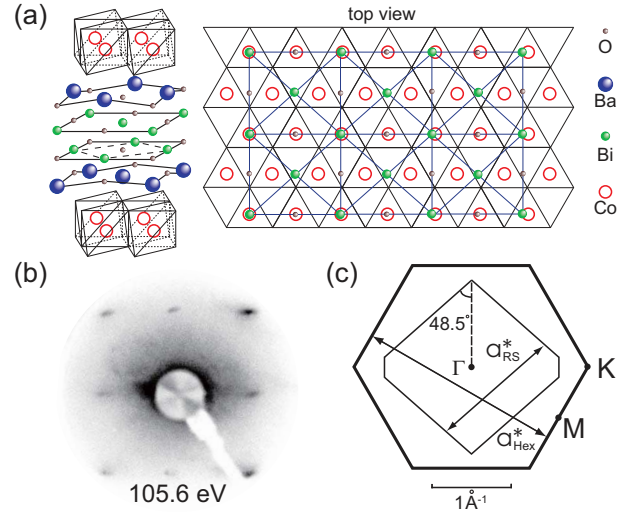


FIG. 1: (color online). (a) A schematic picture of the crystal structure of $\text{Bi}_2\text{M}_2\text{Co}_2\text{O}_y$ ($M = \text{Ca}, \text{Sr}, \text{Ba}$). The oxygen atoms in the CoO_2 layers, and BaO layer in the topview are omitted for simplicity. (b) Low-energy electron diffraction pattern exhibits the four-fold symmetry of the orthorhombic BiO surface of $\text{Bi}_2\text{Ba}_{1.3}\text{K}_{0.6}\text{Co}_{2.1}\text{O}_y$. (c) The reduced Brillouin zones (BZ) for the rocksalt [BiO/BaO] layers (thin lines) and the hexagonal CoO_2 layer (thick lines). The corresponding reciprocal lattice constants a_{RS}^* and a_{Hex}^* are also illustrated.

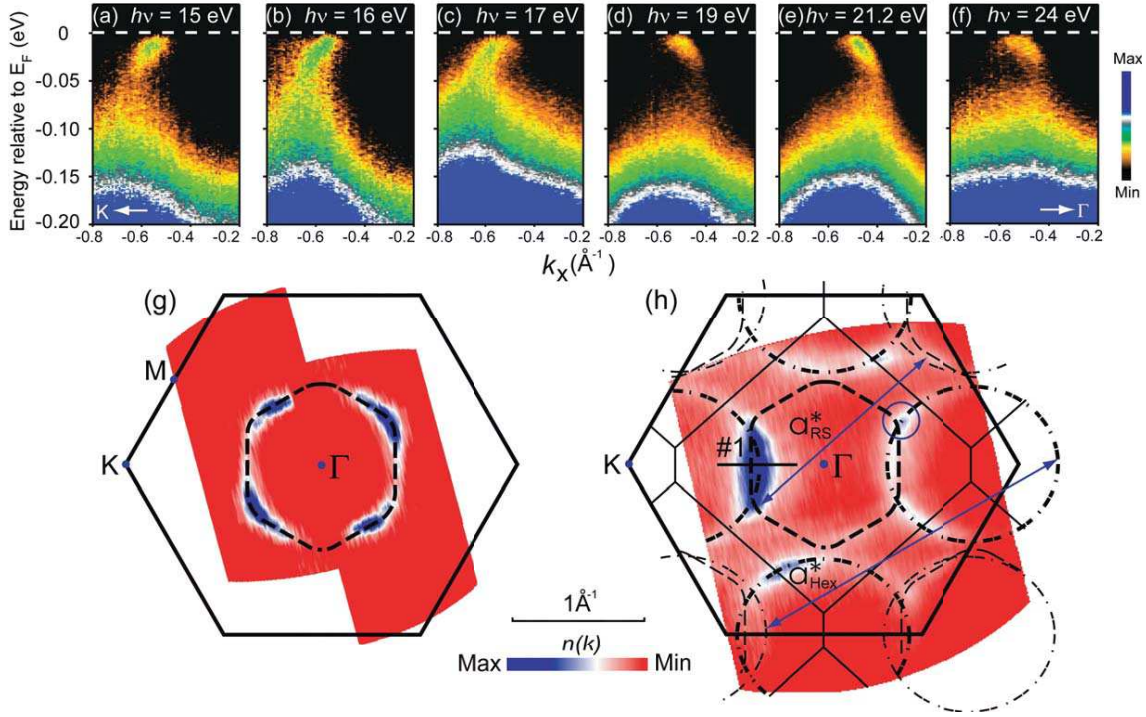


FIG. 2: (color online). ARPES data for $\text{Bi}_2\text{Ba}_{1.3}\text{K}_{0.6}\text{Co}_{2.1}\text{O}_y$ along the cut #1 direction with different photon energies: (a) $h\nu = 15$ eV, (b) $h\nu = 16$ eV, (c) $h\nu = 17$ eV, (d) $h\nu = 19$ eV, (e) $h\nu = 21.2$ eV, (f) $h\nu = 24$ eV. (g-h) Fermi Surfaces measured at 20K with 15 eV and 21.2 eV photons respectively, obtained by integration of the spectral weight in a 20meV window around E_F . The dash-dotted and dashed thick curves are $[\text{CoO}_2]$ -derived and $[\text{BiO}/\text{BaO}]$ -derived Fermi pockets respectively. Their umklapp Fermi surfaces are indicated by thinner curves.

Sr, Ba, Bi) and one CdI_2 -type hexagonal CoO_2 layer with edge-shared CoO_6 octahedra, *e.g.*, $[\text{BaO}]_2[\text{BiO}]_2[\text{CoO}_2]_\alpha$ as shown in Fig.1(a). The two sublattices of rocksalt (RS) layers and hexagonal layer possess incommensurate lattice constants along one Bi-O-Bi axis, and a commensurate one along the other, causing large strain and a global mismatch of the two lattices.

In this Letter, we report ARPES measurements of a misfit structured oxide, $\text{Bi}_2\text{Ba}_{1.3}\text{K}_{0.6}\text{Co}_{2.1}\text{O}_y$ (BBKCO), which reveals the detailed electronic structure of an oxide interface for the first time. We find that large strain in the rocksalt layer significantly raise its chemical potential and induces a large electron transfer to the less strained CoO_2 layer. At the presence of two incommensurate crystal fields, the low energy electronic states of each individual layer are confined within itself, preserving its symmetry; but they undergo umklapp scattering by the incommensurate crystal field from the neighboring layer. Furthermore, a novel interfacial enhancement of electron-phonon interactions (likely with interfacial phonons) is discovered. These novel electronic properties observed in oxide interface depict a detailed microscopic picture of various important processes that could occur at oxide interfaces in general, and provide a foundation for the future design of oxide-based devices.

$\text{Bi}_2\text{Ba}_{1.3}\text{K}_{0.6}\text{Co}_{2.1}\text{O}_y$ possesses the highest thermoelectric power and high conductivity in its class, and thus high figure of merit for thermoelectric applications. The single crys-

tals were prepared by the flux method described in detail elsewhere[19]. Its structure is the same as that in Fig.1(a), with K^+ ions doped into the BaO layer. The two adjacent BiO layers are weakly bound by the van der Waals force, providing a stable BiO natural cleavage plane. This is shown by the rectangular low energy electron diffraction (LEED) pattern in Fig.1(b). The $[\text{BiO}/\text{BaO}]$ layers are orthorhombic, the lattice constants along the two Bi-O-Bi bond directions are $a_{RS} = 5.031$ Å, $b_{RS} = 5.683$ Å respectively. a_{RS} matches the distance between the neighboring Co ions along the same direction, while for the perpendicular direction, $b_{RS} = 1.97 b_{\text{CoO}_2}$, which is collinear but aperiodic, causes the global misfit of the lattice. The CoO_2 sublattice preserves the structure of its free standing form, close to that in Na_xCoO_2 [20]. However, the $[\text{BiO}/\text{BaO}]$ sublattice is largely distorted compared with the BiO, BaO layers in cuprate superconductors $\text{Bi}_2\text{Sr}_2\text{CaCu}_8\text{O}_{8+\delta}$ and $\text{YBa}_2\text{Cu}_3\text{O}_{7-x}$: it is squeezed by 6.4% along the a_{RS} direction, while elongated by about 5.75% along the b_{RS} direction. The Ba^{2+} ions are further displaced from the BaO plane towards the oxygen ions of the CoO_2 layer by 0.4Å. These huge displacements and the misfit indicate large strain in the rocksalt layer. The reduced Brillouin zones for the individual $[\text{BiO}/\text{BaO}]$ layers and CoO_2 layer are plotted in Fig. 1(c).

ARPES measurements were performed at beam line 9 of Hiroshima Synchrotron Radiation Center, beam line 5-4 of Stanford Synchrotron Radiation Laboratory (SSRL), and

beam line 21 of National Synchrotron Radiation Research Center. The first two beamlines are equipped with a Scienta R4000 analyzer, while the latter is equipped with a SES200 analyzer. Typical energy and angular resolutions are 10 meV and 0.3° respectively in the experiments. The samples were cleaved/measured in ultra-high vacuum ($\sim 5 \times 10^{-11}$ mbar).

Two kinds of states with distinct photon energy dependence are identified for BBKCO. Fig. 2(a-f) show the photoemission intensity along the Γ -K direction taken with six different photon energies between 15 eV and 24 eV. With relatively low energy photons [Fig. 2(a-c)], photoemission data show only one feature that disperses towards K at higher binding energies. Correspondingly, the map of photoelectron intensity at the Fermi energy (E_F) gives a hexagonal hole-type Fermi pocket centered around Γ in Fig. 2(g) (dashed lines). This resembles the Fermi surface observed in Na_xCoO_2 [21], whose six-fold symmetry clearly demonstrates its CoO_2 origin. With higher energy photons, another feature that disperses to the opposite direction becomes dominant [Fig. 2(d-f)]. Correspondingly in Fig. 2(h), four hole-type Fermi pockets show up in the intensity map measured at 21.2 eV, which could be fitted with the four dash-dotted ellipses. These Fermi surfaces with the symmetry of the rocksalt layer were not observed in previous ARPES works of other misfit cobaltites[22, 23]. Clearly, they should be mostly originated from the [BiO/BaO] layers. As will be shown later, the observation of the low energy electronic states in both layers enables us to unveil various interfacial effects.

The van der Waals bond between two neighboring BiO layers suggests weak inter-unit-cell coupling. Consistently, the Fermi crossing momenta (k_F 's) in Fig. 2(a-f) show negligible dependency on the photon energies, which samples different out-of-plane momenta k_z 's. For a two dimensional state, one can estimate its occupancy through the Fermi surface volume based on the Luttinger theorem, which robustly holds even in the presence of strong electron correlation and/or electron-phonon interaction[24]. The CoO_2 layers are usually stoichiometric, which would be half filled in undoped case. The actual Fermi surface volume indicates that each CoO_2 formula unit has 0.6 extra electrons. Like in Na_xCoO_2 , the excess carriers come from outside, *i.e.*, the [BiO/BaO] layers here. The [BiO/SrO] layers in cuprate superconductors are prototypical charge reservoir, which donate holes to the CuO_2 plane. Similarly, one would expect [BiO/BaO] layers to donate holes, especially when its Ba^{2+} ions are replaced with K^+ ions. However, in $\text{Bi}_2\text{Ba}_{1.3}\text{K}_{0.6}\text{Co}_{2.1}\text{O}_y$, the Fermi surface volume of the [BiO/BaO] rocksalt layers indicates that 0.6 *electrons* are missing for each [BiO/Ba_{0.65}K_{0.3}Co_{0.05}O] formula unit, which exactly matches the additional electrons in the CoO_2 layer. This large electron (instead of hole) loss out of the [BiO/BaO] layers clearly demonstrates that, when huge strain is present, it would significantly raise the energy of electronic states, and consequently, the electrons flow into the low energy states of the nearby layer. For BBKCO, this charge transfer would save the total energy by hundreds of milli-electronvolt per chemical formula, and thus greatly stabilize the misfit structure.[25]

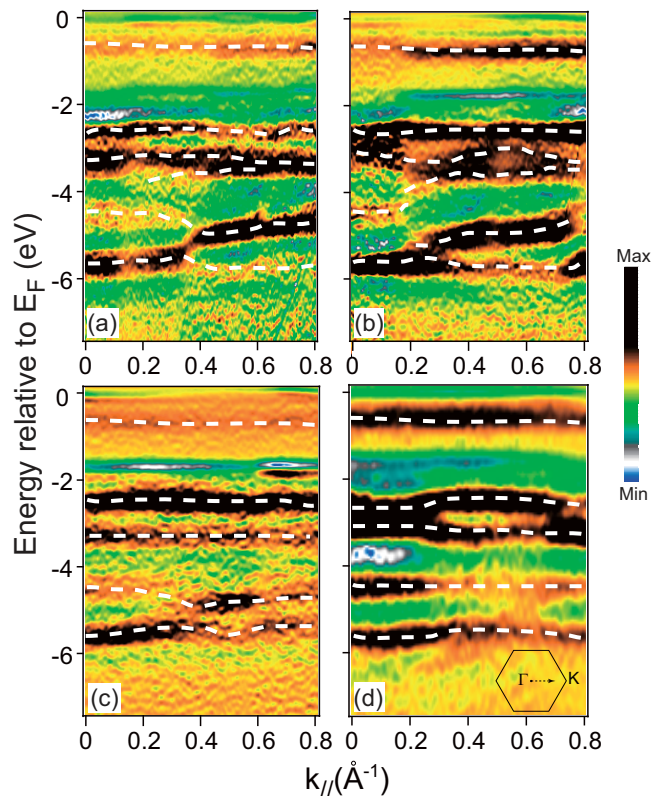


FIG. 3: (color online). Valence band structure determined by taking 2nd derivative of the photoemission intensity along the Γ -K direction taken with (a) 17 eV, (b) 21.2 eV, (c) 28 eV, and (d) 35 eV photons respectively. The dashed lines are identified band structure.

A charge transfer of $0.6e^-$ would induce a Madelung potential as large as 24eV based on simple electrostatic calculation[26]. Therefore, this unrealistic potential must be screened by a “back-flow” of electrons of similar magnitude at the valence bands[27]; in other words, there is covalent bonding across the interface. The evidence for such covalent bonding is indeed found for high-lying states in their dispersion along the out-of-plane dispersion. Fig. 3 shows the valence band dispersion taken along the Γ -K direction for different k_z 's with four different photon energies. Six bands are discernible in total, and the dispersions of bands below -2 eV all display some variations with k_z , with the largest dispersion of about 0.5 eV. These bands are mainly of Ba, Bi and Oxygen character based on a band structure calculation[28]. This k_z dispersion is quite remarkable, since it shows the long range coherence along the c -axis is robust despite that the misfit would cause the bond angle and length to vary along c axis. In the end, for a realistic Madelung potential difference of 1~2eV between layers, the *net* charge difference across the interface would be less than $0.025\sim 0.05 e^-$.

Large charge transfer might allude to strong couplings between two layers, and consequently, bands in different layers would hybridize. Particularly, signatures of band hybridization would show up in the vicinity where their Fermi sur-

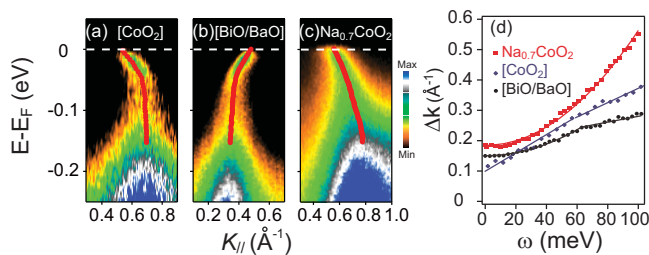


FIG. 4: (color online). Photoemission intensity along $\Gamma - K$ taken at 20K, for (a) BBKCO's CoO₂ layer ($h\nu=15\text{eV}$), (b) BBKCO's [BiO/BaO] layers ($h\nu=21.2\text{eV}$), and (c) Na_{0.7}CoO₂ ($h\nu=21.2\text{eV}$). The thick curves are fitted dispersions. (d) The width of the momentum distribution curve vs. binding energy for data presented in panel a-c, which is an estimate of the quasiparticle scattering rate.

faces cross. On the contrary, we found that in Fig.2(h) the CoO₂ Fermi surface crosses the rocksalt layer Fermi surface without any sign of anti-crossing or bending. In particular, there is even a slight enhancement of spectral weight at the crossing momentum, as highlighted by the thin solid circle. The observed two independent Fermi surface sets with distinct symmetries prove that the low energy electronic states of [BiO/BaO] or CoO₂ layer are spatially confined within itself. This interesting finding is further evidenced by the detailed properties of the quasiparticles. Fig.4(a-b) show the photoemission images of the quasiparticles in the CoO₂ layer, and the [BiO/BaO] layers respectively along the $\Gamma - K$ direction. As shown in Fig.4(d), the measured quasiparticle scattering rate is a linear function of the binding energy for CoO₂ state, while it is a quadratic function near E_F for [BiO/BaO] state. The absence of hybridization between states in two metallic layers of such an oxide interface is quite unexpected, and very different from the strong hybridization observed for quantum well states at metal/semiconductor interfaces[29].

Very interestingly, although the coupling between the low energy electronic states are weak, interlayer interactions could still manifest themselves in other forms, for example, in the several weak Fermi surfaces (thin lines) in Fig.2(h). If one would displace the main Fermi surface of [BiO/BaO] layers by the reciprocal lattice constant a_{Hex}^* of the CoO₂ layer (illustrated by the double-headed arrows), the resulting umklapp Fermi surfaces perfectly fit the weak features in the data. Similarly, the CoO₂ umklapp Fermi surfaces are observed apart from the main ones by the reciprocal lattice constant a_{RS}^* of the [BiO/BaO] layers. Therefore, this observation proves that the crystal field from one side of the interface is imposed on the other, and act as an incommensurate potential that scatters the electrons there.

More interfacial effects could be revealed by comparing the BBKCO data with the quasiparticle behavior of Na_{0.7}CoO₂ taken in the same momentum region. While the Na_{0.7}CoO₂ dispersion is a smooth curve [Fig.4(c)], there are strong kinks on the dispersions of the BBKCO bands [Fig.4(a-b)]. These kinks are signature of interaction with some bosonic modes, most likely phonons here, considering the non-magnetic na-

ture of the rocksalt layer. The similar energy scale of 60 meV for both CoO₂ and [BiO/BaO] states indicates they might interact with the same phonons induced at the highly strained interface. This strong coupling to a mode is also reflected in its scattering rate [Fig.4(d)], where a clear turning point around 60meV appears for both the bands of BBKCO. Furthermore, the scattering rate of Na_{0.7}CoO₂ is a simple quadratic function of binding energy, different from the linear behavior of the BBKCO CoO₂ layer. This suggests that the electron-phonon interactions induced by the interface may change the quasiparticle behavior.

The current findings for an oxide interface provide some important guidelines for future device design. For example, our results suggest that interfacial strain might cause large charge transfer without severely changing the properties of participating layers, since the coupling between the low energy electronic states could still be weak. Meanwhile, the interfacial umklapp scattering and phonon effects might alter the low energy electronic behavior.

To summarize, we have revealed various interfacial electronic properties that have never been observed in oxide interfaces before. We show that while the low energy states are confined within individual layer, the high lying states are covalently coupled. The relation between strain and charge transfer across oxide interface is illustrated from a microscopic level. The enhancement of electron phonon coupling and interfacial umklapp scattering are discovered. Our findings provide an electronic structure foundation for understanding oxide interfaces and designing oxide devices.

We gratefully acknowledge the experimental help from Dr. D. H. Lu, and R. H. He during the SSRL experiment, and the helpful discussions with Profs. Z.-X. Shen, C. Kim, Z. Q. Wang and Dr. T. Cuk. This work was supported by NSFC, MOST (973 projects No.2006CB921300 and 2006CB922005), and STCSM of China. Portions of this research were carried out at SSRL, a national user facility operated by Stanford University on behalf of the U.S. DOE, Office of BES.

* Electronic address: dlheng@fudan.edu.cn

- [1] A. Ohtomo, H. Y. Hwang, *Nature* **427**, 423 (2004).
- [2] N. Reyren *et al.*, *Science* **317**, 1196 (2007).
- [3] K. Ueda, H. Tabata, T. Kawai, *Science* **280**, 1064 (1998).
- [4] N. Nakagawa, H. Y. Hwang, and D. A. Muller, *Nature Materials* **5**, 204 (2006).
- [5] J. Chakhalian *et al.*, *Science* **318**, 1114 (2007).
- [6] A. Tsukazaki *et al.*, *Science* **315**, 1388 (2007).
- [7] S. Altieri, L. H. Tjeng, and G. A. Sawatzky, *Phys. Rev. B* **61**, 16948 (2000).
- [8] H. Ohta *et al.*, *Nature Mater.* **6**, 129 (2007).
- [9] S. B. Ogale, *Thin Films and Heterostructures for Oxide Electronics* (Springer Verlag, Berlin, 2005).
- [10] J. Voit *et al.*, *Science* **290**, 501 (2000).
- [11] J.-P. Locquet *et al.*, *Nature* **394**, 453 (1998).
- [12] S. Okamoto and A. J. Millis, *Nature* **428**, 630 (2004).

- [13] H. Kumigashira *et al.*, Appl. Phys. Lett. **84**, 5353 (2004).
- [14] M. Takizawa *et al.*, Phys. Rev. Lett. **97**, 057601 (2006).
- [15] K. Maekawa *et al.*, Phys. Rev. B **76**, 115121 (2007).
- [16] H. Wadati *et al.*, Phys. Rev. B **77**, 045122 (2008).
- [17] A. C. Masset *et al.*, Phys. Rev. B **62**, 166 (2000).
- [18] H. Leligny *et al.*, C. R. Sci. Paris IIc, Chim **2**, 409 (1999).
- [19] X. G. Luo *et al.*, J. Phys.: Condens. Matter **20**, 215221 (2008).
- [20] I. Terasaki, Y. Sasago and K. Uchinokura, Phys. Rev. B **56**, R12685 (1997).
- [21] H. B. Yang *et al.*, Phys. Rev. Lett. **95**, 146401 (2005).
- [22] Z. Yusof *et al.*, Phys. Rev. B **76**, 165115 (2007).
- [23] V. Brouet *et al.*, Phys. Rev. B **76**, 100403(R) 2007.
- [24] D. W. Shen *et al.*, Phys. Rev. Lett. **99**, 216404 (2007).
- [25] The energy saved through charge transfer can be roughly estimated to be $v_F^0 \times \Delta k$, where $v_F^0 \approx 1.4eV\text{\AA}$ is the bare band velocity of the rocksalt layer, and $\Delta k \approx 0.35\text{\AA}^{-1}$ is the difference of [BiO/BaO] Fermi pocket radius before and after the charge transfer.
- [26] W. H. Xie, O. Jepsen, O. K. Andersen, Y. L. Chen, and Z.-X. Shen, Phys. Rev. Lett. **98**, 047001 (2007).
- [27] Z.-Y. Lu, G. L. Chiarotti, S. Scandolo and E. Tosatti, Phys. Rev. B **58**, 13698 (1998).
- [28] Y. Zhu, Z. Q. Yang, (in preparation).
- [29] S.-J. Tang, Y.-R. Lee, S.-L. Chang, T. Miller, and T.-C. Chiang, Phys. Rev. Lett. **96**, 216803 (2006).